Journal of Membrane Science 428 (2013) 546–553

Contents lists available at SciVerse ScienceDirect

Journal of Membrane Science

journal homepage: www.elsevier.com/locate/memsci

Water-solubility-driven separation of gases using graphene membrane

Joonho Lee, N.R. Aluru *

Department of Mechanical Science and Engineering, Beckman Institute for Advanced Science and Technology, University of Illinois at Urbana-Champaign, Urbana, IL 61801, USA

ARTICLE INFO

Article history:
Received 5 May 2012
Received in revised form
28 September 2012
Accepted 2 November 2012
Available online 10 November 2012

Keywords:
Gas separation
Molecular dynamics
Graphene

ABSTRACT

We investigate separation of gas-mixtures using a graphene membrane. By introducing a water slab between a gas-mixture and the graphene membrane, we show that the gas-mixture can be separated based on the water-solubility of the gas molecule. By considering various gas-mixtures we show that the separation ratio follows the water-solubility ratio of the gas molecules in the mixture. We also demonstrate the water-solubility-driven separation of gas-mixtures using a carbon nanotube, but we show that the graphene membrane provides higher selectivity ratio because of its single-atom thickness.

1. Introduction

Separation of CO_2 from the flue gas is an important step towards reducing the global emissions of CO_2. Many processes such as adsorption, absorption and membrane technology have been used to remove CO_2 from the flue gas [1,2]. A popular industrial method to separate CO_2 is to use amine solvents in the absorption process. In spite of high product yields and purities, high energy consumption and liquid loss in desorption are regarded as disadvantages of the approach [2,3]. On the other hand, membrane technology has been considered as an energy efficient method for CO_2 separation for a couple of decades, as membranes are thin and easy to scale-up [4]. Recent studies on gas separation through membranes have focused on inorganic membranes such as zeolites and carbon-based membranes for high-temperature environments [5–8]. The thickness of these membranes ranges from tens of nanometers to several micrometers.

Taking advantage of both the absorption and the membrane technologies, a couple of methods have been proposed. The first one is a membrane contactor in which a membrane acts as an interface between the feed gas and the absorption liquid [9,10]. CO_2 is solvated in the absorption liquid through the membrane and this solvated CO_2 is separated later by using stripper or the same type of membrane contactor called desorber [11]. The second approach uses a liquid membrane, where an absorption liquid and polymeric membranes are placed between two gas regions. CO_2 in the feed gas region penetrates through the liquid membrane and comes out to the other region [12]. Ever since the liquid membrane (or membrane contactor) was introduced [13,14], separation methods based on the absorption liquid and the membrane have improved over a couple of decades and researchers have primarily focused on various systems and diverse materials in the liquid membrane system. To achieve efficient gas separation through the liquid membrane, the type of absorption liquid used in the system is important. Water as an absorption liquid has steadily received much attention for gas separation [11,15,16]. In addition, different materials for the membrane have been used instead of the conventional polymeric membrane, to reduce the overall diffusion thickness.

Graphene is a promising material for various applications because of its exceptional physical properties and atomic scale thickness [17]. Graphene is a single-atom-thick planar sheet made of carbon atoms arranged in a hexagonal lattice. Graphene, without defects, does not have pores and is impermeable, but atomic scale pores can be generated in a graphene sheet by chemical or thermal treatment [18,19]. Porous graphene has been investigated as a membrane material and it has been shown to be a fast transporter of water [20]. In addition, porous graphene has also been shown to be a high performance membrane material for ion, gas and nanoparticle separation [21–23]. Jiang et al. considered graphene with subnanometer size pores as a membrane for gas separation and observed that porous graphene can be a highly efficient membrane for gas separations [22].

In this paper, we investigate water solubility-driven separation of CO_2 from CO_2/O_2, CO_2/N_2 and CO_2/CH_4 mixtures using a porous graphene membrane. Molecular dynamics simulation is an important tool to understand the vapor–liquid and liquid–solid interface effects on the separation procedure and the coupled interaction of gas with the graphene pore and the water slab [24].

* Corresponding author. Tel.: +1 217 333 1180; fax: +1 217 244 4333.
E-mail address: aluru@illinois.edu (N.R. Aluru).
URL: http://netfiles.uiuc.edu/aluru/www/ (N.R. Aluru).

0376-7388/$ - see front matter © 2012 Elsevier B.V. All rights reserved.
http://dx.doi.org/10.1016/j.memsci.2012.11.006

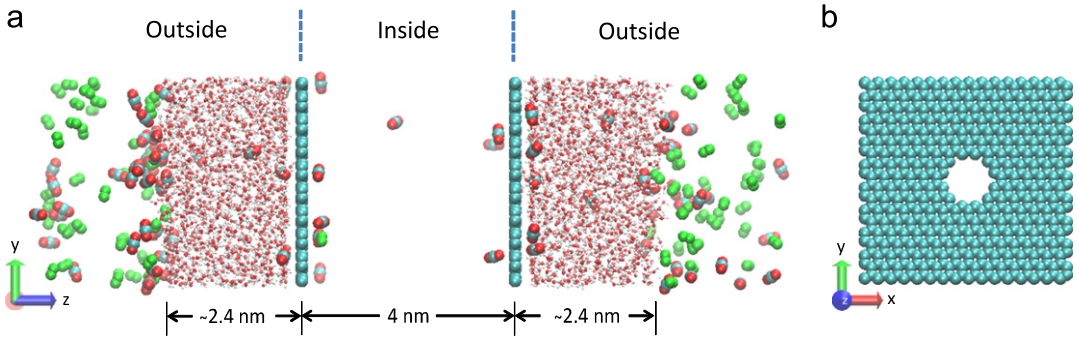

Fig. 1. (a) Snapshot of the system (CO_2/O_2 separation though water/graphene membrane). (b) Porous graphene membrane.

By performing extensive molecular dynamics simulations, we understand separation of gases. To investigate the merits of porous graphene for gas separations, we also perform molecular simulations using carbon nanotubes (CNT). Studies on CNT have shown fast transport of water and gases through the tubes [25–27], so comparison studies between porous graphene and CNT can provide insights on the effect of the length of the pore on gas separations. We envision that our work will lead to the use of porous graphene as an efficient membrane for gas separations.

2. Methods

We performed molecular dynamics simulations to investigate water solubility-driven separation of gases through a porous graphene membrane. A snapshot of the CO_2/O_2 mixture and the water slab separating the mixture and the porous graphene membrane is shown in Fig. 1(a). The volume of the system ($3.9 \times 3.8 \times 14.0\ nm^3$) is fixed throughout the simulation. The gas mixture is initially positioned at both ends of the system. During simulation, the gas molecules penetrate through the water slab and the porous graphene membrane and enter into the middle region, which is initially empty. The 0.99 nm diameter graphene pore is shown in Fig. 1(b). The thickness of the water slab is approximately 2.4 nm. The bond length of CO_2, O_2 and N_2 is maintained by the shake constraint scheme. The bond stretching and angle bending of CH_4 is controlled by the OPLS-AA force field [28]. The non-bonded potential energy between molecules is given by

$$U_{nonbond} = U_{LJ} + U_{Coulomb} \tag{1}$$

where

$$U_{LJ} = \sum_{i,j} 4\epsilon \left[\left(\frac{\sigma_{ij}}{r_{ij}} \right)^{12} - \left(\frac{\sigma_{ij}}{r_{ij}} \right)^{6} \right] \tag{2}$$

$$U_{Coulomb} = \sum_{i,j} \frac{q_i q_j}{r_{ij}} \tag{3}$$

The Lennard–Jones (L–J) and Coulomb potential parameters for the various gas molecules (CO_2, O_2, N_2 and CH_4) are taken from [28–30]. We estimated the solubility of CO_2 [29,31,32], O_2 [30,33,34], N_2 [29,30,33] and CH_4 models [28,35] by the method discussed in Ref. [36] using SPC/E water slab at 300 K. The models used in this work for CO_2, O_2, N_2 and CH_4 show the closest solubility of each gas in water to experimental data at 300 K. For water, SPC/E model is used [37]. The porous graphene membranes are positioned at $z=5$ nm and $z=9$ nm. The force-field parameters for the carbon atom of the graphene membrane are taken from [38]. The L–J parameters between different molecules were obtained by applying the Lorentz–Berthelot mixing rules, $\sigma_{ij} = (\sigma_{ii} + \sigma_{jj})/2$ and $\epsilon_{ij} = \sqrt{\epsilon_{ii}\epsilon_{jj}}$. A cut-off distance of 1.2 nm is used for the L–J potential. Electrostatic interactions were computed by using the Particle Mesh Ewald method with a grid spacing of 0.15 nm. Periodic boundary conditions are applied in all the three directions. Time integration was performed by using the leap-frog algorithm with a time step of 1.0 fs. The temperature of the system is maintained at 300 K by Nosé–Hoover thermodynamics with a characteristic time of 0.1 ps [39]. Simulations were performed using GROMACS 4.0.7 [40].

3. Results and discussion

3.1. Solubility of gases in water

Before presenting results on the separation of gases through the porous graphene membrane, we discuss the solubility of the various gases considered in this work (CO_2, O_2, N_2 and CH_4) in bulk water at 300 K. The solubility results will not only explain the separation properties, but also show the limitations, if any, of the force-fields in accurately representing experimental solubility data. We estimated the solubility of each gas using the method discussed in [36]. We simulated the water slab system, as shown in Fig. 2(a), with 98 gas molecules and 1600 water molecules at 300 K. Using the averaged value of gas concentration along the z-axis, as shown in Fig. 2(b), we calculated gas concentration in the water slab. Since the concentration of gas in water is proportional to gas vapor pressure, we can compare the gas solubility by calculating the Henry's constant (pressure unit) as shown in Table 1. The gas vapor pressure is calculated by van der Waals equation and Henry's constant is calculated based on Henry's law $h_H = p/x$, where p is the pressure of gas in the vapor region and x is the mole fraction of gas in the water slab. If the gas molecule has a smaller Henry's constant, then it has a higher solubility. We note that CO_2 has higher solubility compared to that of O_2, N_2 and CH_4. The solubility of O_2 is about two times bigger than that of N_2 and the solubility of CH_4 is between that of O_2 and N_2. Even though there is some discrepancy between experimental solubilities and our estimated values, the ratios of various gas solubilities are reasonable compared to the experimental values and we will use this to explain gas separations.

3.2. Separation of gas mixtures

As shown in Fig. 1(a), the computational domain for gas separations is divided into inside and outside regions. The separation of gas molecules is identified by the number of the gas molecules in the inside and outside regions as a function of the simulation time. Initially, the gas mixtures are positioned in the outside region, next to the water slab. The gas molecules diffuse through the water slab and through the porous graphene membrane to the inside region. To demonstrate the significance

of solubility-driven separation of gases, we also simulated graphene-only case, where the system setup is similar to Fig. 1, except that the water slab is not present.

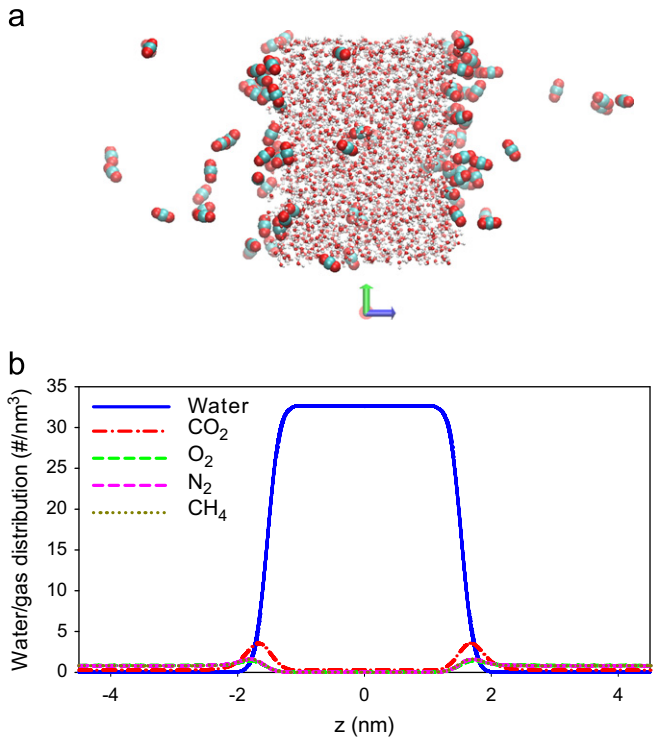

Fig. 2. (a) Snapshot of the system for solubility calculation. (b) Water and gas concentrations of the system along the *z*-axis.

Table 1
Solubility and Henry's constant of CO_2, O_2, N_2 and CH_4.

Gas	Solubility (mole fraction *x*)	Pressure (MPa)	Henry's constant (MPa)	Ref. Henry's constant (MPa)
CO_2	8.0×10^{-3}	1.1	1.5×10^{2}	1.4×10^{2}
O_2	6.3×10^{-4}	3.4	4.3×10^{3}	5.4×10^{3}
N_2	2.7×10^{-4}	3.3	9.7×10^{3}	1.2×10^{4}
CH_4	5.1×10^{-4}	3.3	5.8×10^{3}	4.2×10^{4}

The simulation results for the CO_2/O_2 mixture are shown in Fig. 3, for the CO_2/N_2 mixture in Fig. 4, and for the CO_2/CH_4 mixture in Fig. 5. The separation of gases in the absence of the water slab are also shown in these figures. In the case of graphene-only simulations (no water slab), equilibration is achieved within 3 ns and the number of gas molecules in the inside and the outside regions fluctuate around a fairly constant value. In the absence of the water slab, we note that for the various gas mixtures, the other gas molecule (O_2, N_2 and CH_4) passes through the graphene nanopore slightly faster than the CO_2 molecule. In this case, the size of the gas molecule relative to the size of the nanopore is important for gas selectivity. In the case of a 0.99 nm diameter graphene pore without the water slab, no significant selectivity or separation of the gas molecules is achieved for the various gas mixtures considered. Compared to the graphene-only case, in the presence of a water slab, as shown in Figs. 3(b), 4(b), and 5(b), a significant separation of gas molecules is observed. In particular, we observed that highly soluble CO_2 molecules are selectively transported through the water/graphene membrane and other gas molecules such as O_2, N_2 and CH_4 having low solubility in water hardly penetrate through the water/graphene membrane.

The flux of each gas molecule and the selectivity of CO_2/O_2, CO_2/N_2 and CO_2/CH_4 gas mixtures through the water/graphene membrane system are shown in Table 2. In the CO_2/O_2 case, the flux of CO_2 is about 9.5 times higher than the flux of O_2. The flux of N_2 in the CO_2/N_2 mixture is lower than the flux of O_2 in the CO_2/O_2 mixture and this reduction of N_2 flux through the water/graphene membrane causes higher selectivity of CO_2 for the CO_2/N_2 mixture than CO_2 from the CO_2/O_2 mixture. Higher CO_2 selectivity in the CO_2/N_2 mixture is consistent with the higher solubility ratio of CO_2/N_2 compared to that of CO_2/O_2. In the case of CO_2/CH_4 mixture, the selectivity of CO_2 over CH_4 is in between the selectivity of CO_2 over N_2 and CO_2 over O_2. This selectivity of CO_2 from different gas mixtures can be explained by the solubility difference between CO_2 and the other gas molecule (O_2, N_2 and CH_4).

The water slab shown in Fig. 1(a) has two interfaces – vapor/water free interface and the water/graphene interface. Once the gas molecules (mainly CO_2) dissolve in water from the vapor/water interface and pass through the graphene pore to the inside region of the system, they hardly penetrate back to the water slab through the graphene nanopore. This asymmetrical structure of the water/graphene membrane is useful to induce one-directional flux of gas molecules.

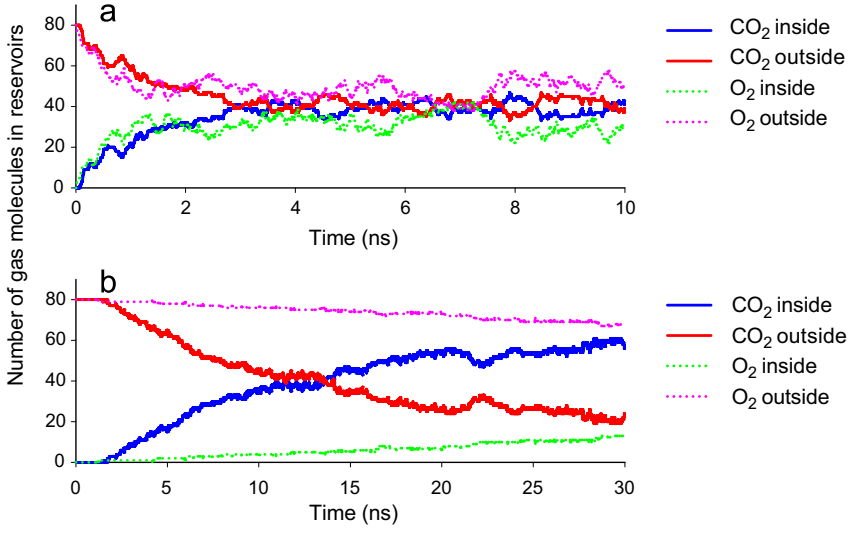

Fig. 3. Gas separation of CO_2/O_2 mixture: (a) number of CO_2/O_2 in inside and outside through the 0.99 nm graphene pore without water; (b) number of CO_2/O_2 in inside and outside through water/graphene membrane.

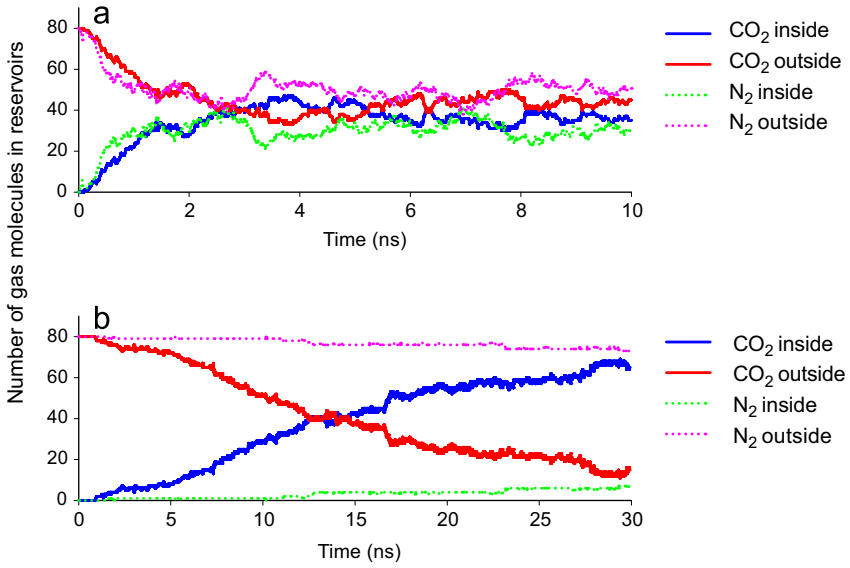

Fig. 4. Gas separation of CO_2/N_2 mixture: (a) number of CO_2/N_2 in inside and outside through the 0.99 nm graphene pore without water; (b) number of CO_2/N_2 in inside and outside through water/graphene membrane.

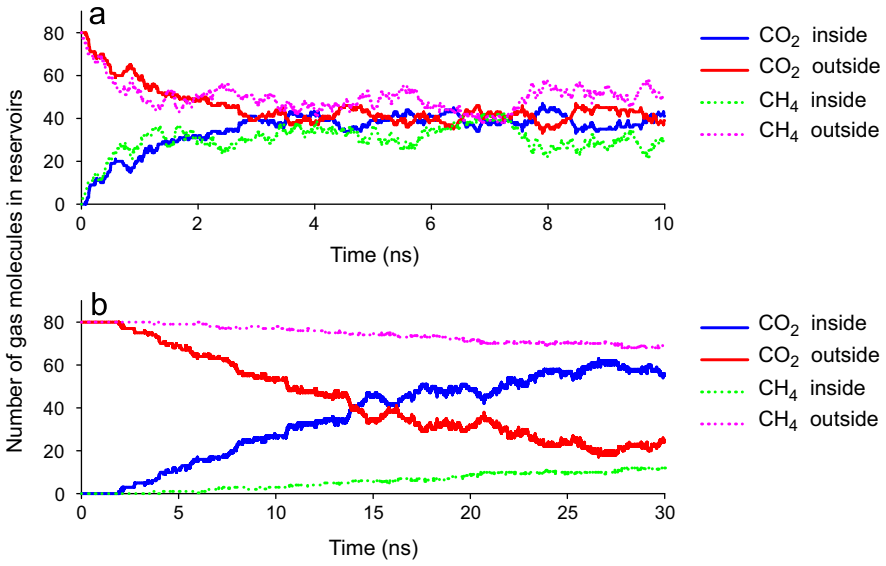

Fig. 5. Gas separation of CO_2/CH_4 mixture: (a) number of CO_2/CH_4 in inside and outside through the 0.99 nm graphene pore without water; (b) number of CO_2/CH_4 in inside and outside through water/graphene membrane.

We also increased the thickness of the water slab from 2.4 nm to 4.2 nm to investigate the effect of water thickness on selectivity. We repeated the simulation of CO_2/O_2 mixture using 4.2 nm water/graphene membrane system. The number of gas molecules in different regions of the system is shown in Fig. 6(b). The flux of both CO_2 and O_2 molecules is smaller than in the 2.4 nm water slab case; the flux of CO_2 molecules is about 2.7 ns^{-1} and the flux of O_2 molecules is about 0.21 ns^{-1}. The increased water slab thickness suppresses the flux of O_2 more than the flux of CO_2 which gives a higher selectivity of about 12.8 compared to 9.5 in the 2.4 nm water/graphene case. As the gas molecules do not penetrate through the thicker water slab easily compared to the thinner water slab and the concentration ratio in water is decided by the solubility, the gas flux through the thicker water slab approaches the solubility ratio between CO_2 and O_2 of 28.7.

During the simulations, no water molecules passed through the graphene pore. This can be explained by the strong interaction between water molecules, which is represented by the hydrogen bonding network. The strong water–water interaction and the relatively smaller interaction with graphene makes the penetration of water molecules through the nonpolar graphene pore difficult [41,42]. However, there is still a chance of water evaporating slowly from the system and water loss could be compensated by a refilling process through the *x*, *y*-directions. To prevent evaporation of the water slab in the water/graphene membrane, another membrane can be used at the free surface of the water slab. For example, a graphene membrane with a larger pore can be used. As shown in Fig. 7,

Table 2
Separation of CO_2 from different gas mixtures with water/graphene membrane.

Gas mixture	CO_2 flux (# of molecules/ns)	Other gas flux (# of molecules/ns)	Selectivity
CO_2/O_2	4.1 ± 0.3	0.43 ± 0.04	9.5 ± 0.7
CO_2/N_2	3.3 ± 0.5	0.23 ± 0.06	14.4 ± 1.4
CO_2/CH_4	4.1 ± 0.5	0.35 ± 0.12	9.9 ± 0.7

a graphene membrane with a larger opening is used at the water/vapor interface to prevent evaporation of water and the inside graphene membrane has a pore of 0.99 nm pore. We investigated separation of the CO_2/O_2 mixture using the system shown in Fig. 7 and compared the results with the previous results. We observed that the separation of CO_2 was not as efficient as in the previous case as shown in Fig. 7(b). However, if we reduce the Lennard–Jones interaction parameter, ϵ, of the outside graphene membrane to

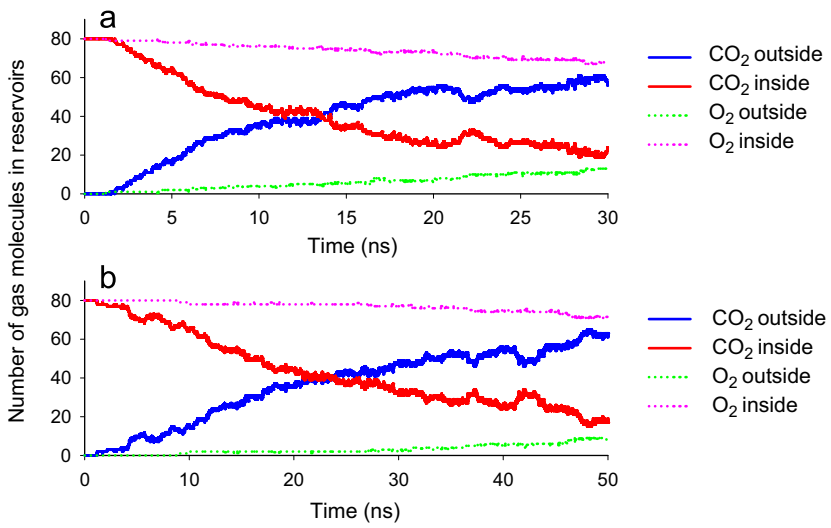

Fig. 6. Gas separation of CO_2/O_2 mixture with different thickness of water: (a) number of CO_2/O_2 in inside and outside through 2.4 nm water/graphene membrane; (b) number of CO_2/O_2 in inside and outside through 4.2 nm water/graphene membrane.

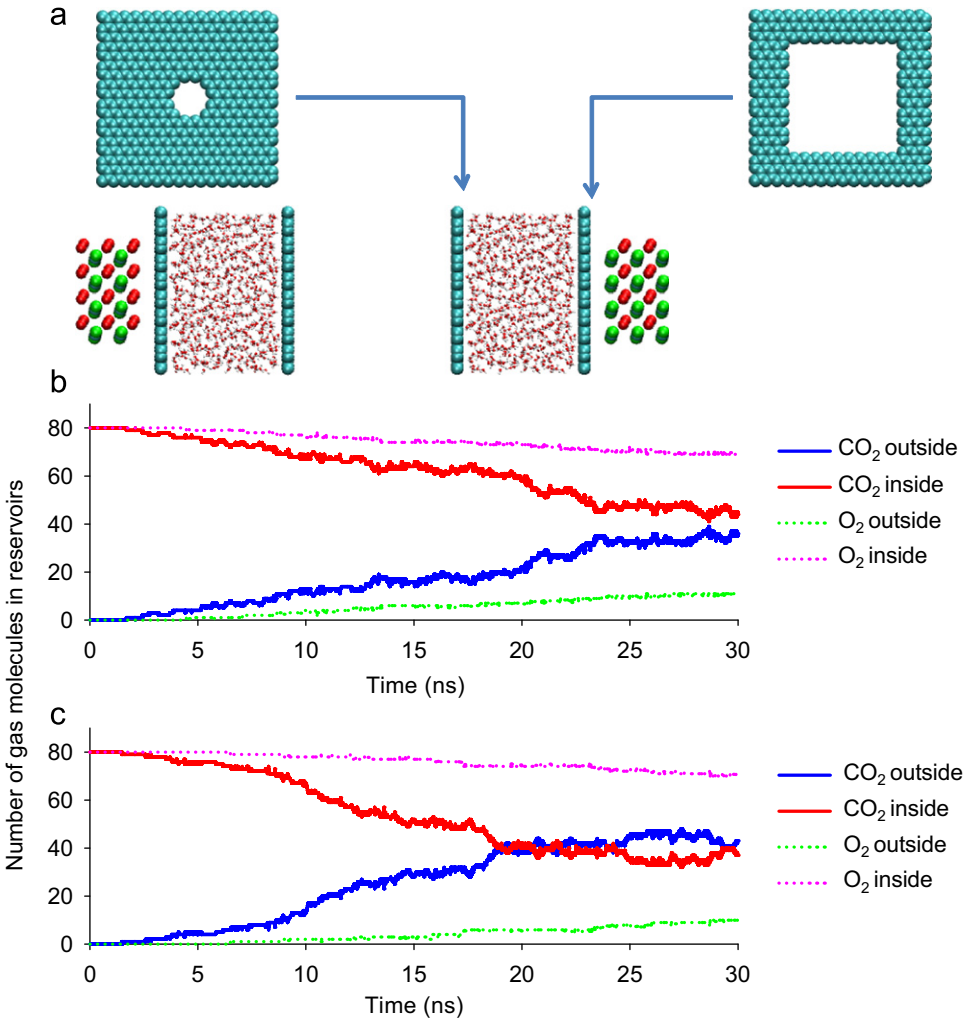

Fig. 7. Gas separation of CO_2/O_2 mixture using a different water/graphene membrane: (a) snapshot of the system; (b) number of CO_2/O_2 molecules in inside and outside regions of the system; (c) number of CO_2/O_2 molecules in inside and outside regions with a reduced ϵ.

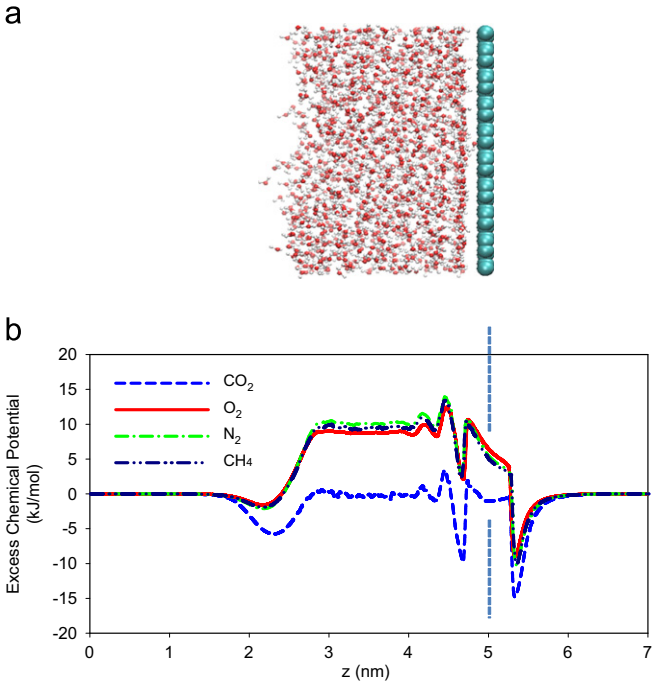

Fig. 8. (a) System (water slab and porous graphene) for calculation of excess chemical potential. (b) Excess chemical potential of CO_2, O_2, N_2 and CH_4 along the z-axis.

Table 3
Excess chemical potential of CO_2, O_2, N_2 and CH_4 in the water membrane.

Gas	Excess chemical potential (kJ/mol)
CO_2	-0.19 ± 0.25
O_2	8.77 ± 0.09
N_2	10.05 ± 0.14
CH_4	9.57 ± 0.16

weaken the interaction between CO_2 and the outside graphene membrane, the penetration of CO_2 through the water/graphene membrane is enhanced as shown in Fig. 7(c). Thus, it is possible to obtain comparable selectivity of CO_2 and prevent the evaporation of water by using an appropriate membrane for the outside region.

3.3. Potential barriers

To further understand the selectivity ratio of gas mixtures, we evaluated the excess free energy of various gas molecules along the z-axis of the system. We performed the simulations at 300 K on water slab and porous graphene, without gas mixtures, as shown in Fig. 8(a) to generate configurations for the Widom insertion method [43,44]. In the Widom insertion method, after inserting a gas molecule at a random position in each configuration of the system, we compute $\exp(-\beta\Delta U)$, where ΔU is the potential energy difference between the systems before and after adding a gas molecule, $\Delta U = U(N_{tot}+N_{gas})-U(N_{tot})$, when $N_{gas}=1$. The excess chemical potential is an average over all the configurations, defined as

$$\Delta\mu_{ex} = -kT \ln \frac{\langle V \int ds_{N+1} \exp(-\beta\Delta U)\rangle}{\langle V\rangle} \quad (4)$$

where k is the Boltzmann constant, T is the temperature of the system, $\beta = 1/kT$, V is the volume of the system, and $\langle \dots \rangle$ indicates an average over all the configurations.

The calculated excess chemical potential variation along the z-axis is shown in Fig. 8(b) and the average chemical potential value of each gas molecule in the water slab region is shown in Table 3. The potential difference of various gas molecules in the water slab region is reasonable and consistent with the solubility difference of gas molecules in water [45]. The chemical potential variation shows that the solubility difference in the water slab drives the selectivity of CO_2 from CO_2/O_2, CO_2/N_2 and CO_2/CH_4 mixtures. In particular, when the gas molecules are near the porous graphene, the chemical potential difference between CO_2 and other gases becomes smaller but still the difference is maintained which can be regarded as a combined effect of water and porous graphene.

3.4. Separations using CNT

To further understand the significance of separations using graphene, we performed gas separations using a carbon nanotube (CNT) and compared its performance with that of graphene. We considered a (13,0) CNT which has a diameter of 1.02 nm (this diameter is similar to the graphene nanopore size of 0.99 nm) and a length of 3 nm. Using the CNT structure as the membrane between vapor and water slab, we performed the simulation on CO_2/O_2 mixture to investigate gas selectivity difference between CNT and graphene pore. Other simulation conditions are identical to the graphene/water slab simulations. The system is again divided into inside and outside regions in CNT/water slab system and the CO_2/O_2 mixture is initially positioned in the outside region as shown in Fig. 9(a). We count the number of CO_2 molecules in both the regions to estimate the separation of CO_2 through the water/CNT membrane system (see Fig. 9(b) and (c)). As the CO_2 molecules enter the CNT from the water slab, they fill the CNT. After a certain amount of CO_2 molecules occupied the CNT (at around $t=10$ ns), CO_2 molecules begin to pass through the CNT and enter the inside region. The number of CO_2 molecules in the CNT increase gradually until the CNT is completely filled with gas molecules. Once the CNT is completely filled at around $t=18$ ns, the instant flux of the CO_2 molecules passing though the water/CNT membrane reduces from 2.5 to 1.3 ns^{-1}. CO_2 filling the CNT reduces the flux of the gas molecules.

To understand this CO_2 behavior, we calculate the interaction energy of various gas molecules with graphene and CNT when the gas molecule is in the middle of the membrane as shown in Fig. 10. Though CO_2 interaction is stronger than O_2, N_2 or CH_4 in both CNT and graphene structures, the interaction energy difference between CO_2 and other gas molecules (O_2, N_2 and CH_4) is larger in CNT than in the graphene pore as shown in Table 4. The strong interaction energy between CO_2 and CNT makes the interior of the CNT a favorable place for CO_2. Therefore, CO_2 molecules are not able to escape easily until high density of CO_2 in the CNT is achieved. The strong interaction between CO_2 and CNT was also reported in Refs. [46,47]. The selectivity ratio of CO_2 over O_2 in the CNT/water slab system is about 7.5 (before filling) and about 3.3 (after filling), which is lower than the selectivity ratio of about 9.5 obtained in the graphene/water slab system. These results indicate that water solubility-driven separation of gases can be observed even in the case of CNT pores, but the length of the pore affects the separation ratio and graphene, because of its single-atom thickness, is ideally suited for water solubility-driven separation of gases. For the separation of other mixtures, CO_2/CH_4 and CO_2/N_2, we performed additional simulations and observed similar gas separation behavior.

4. Conclusions

We have shown that a graphene membrane can efficiently separate CO_2 from CO_2/O_2, CO_2/N_2 and CO_2/CH_4 mixtures.

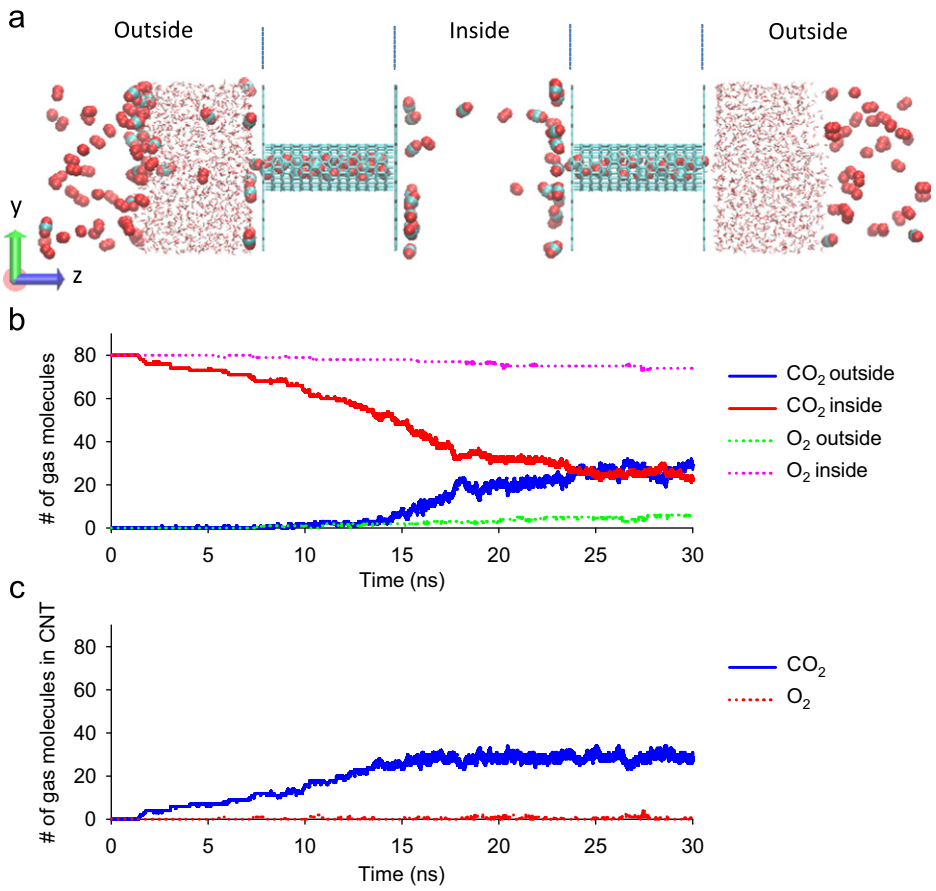

Fig. 9. Gas separation of CO_2/O_2 mixture through water/CNT membrane: (a) snapshot of the system; (b) number of CO_2/O_2 in inside and outside regions; (c) number of CO_2/O_2 molecules in the CNT.

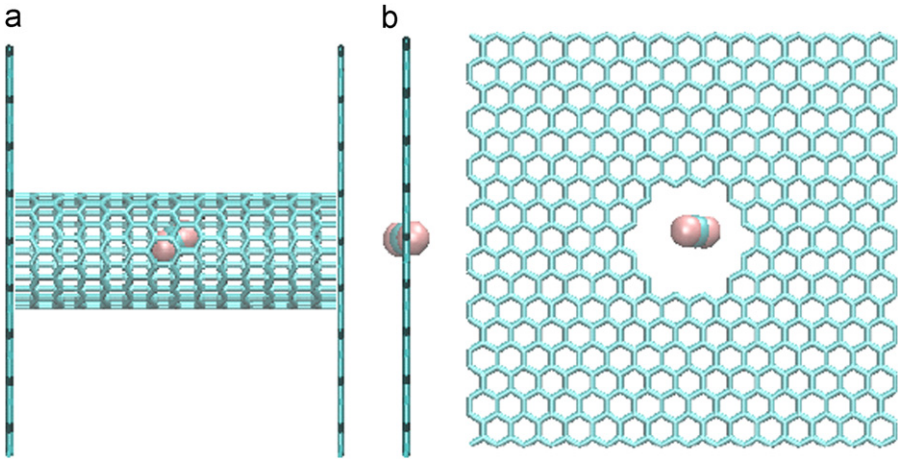

Fig. 10. Configuration for calculation of the interaction energy between a gas molecule and CNT/graphene: (a) configuration of CO_2 in a (13,0) CNT; (b) configuration of CO_2 in the graphene pore.

The separation ratio follows the water-solubility of the gas molecules in the mixture. By investigating the gas mixtures with and without water slab, we have shown that the separation of the gas mixtures can be controlled and the selectivity ratio can be enhanced with the water slab. A thicker water slab, provided a higher selectivity ratio. Even though carbon nanotubes have been shown to be fast transporters of gas and water molecules, we have shown that the graphene membrane, because of its single-atom thick

Table 4
Interaction energy between a gas molecule and CNT/graphene.

Gas	(13,0) CNT (kJ/mol)	Graphene pore (kJ/mol)
CO_2	-31.2 ± 2.3	-9.6 ± 1.3
O_2	-16.4 ± 1.7	-5.1 ± 1.2
N_2	-19.4 ± 1.5	-6.2 ± 1.1
CH_4	-20.8 ± 1.8	-6.5 ± 1.3

length compared to the finite length of the carbon nanotube, provides higher selectivity and faster transport of gas molecules compared to the carbon nanotube.

Acknowledgements

This work was supported by the National Science Foundation (NSF) under Grants 0328162 (nano-CEMMS, UIUC), 0852657, 0915718, and 0941497.

References

[1] M. Freemantle, Membranes for gas separation, Chem. Eng. News 83 (2005) 49–57.
[2] H. Yang, Z. Xu, M. Fan, R. Gupta, R.B. Slimane, A.E. Bland, I. Wright, Progress in carbon dioxide separation and capture: A review, J. Membr. Sci. 20 (2008) 14–27.
[3] D.M. D'Alessandro, B. Smit, J.R. Long, Carbon dioxide capture: prospects for new materials, Angew. Chem. Int. Ed. 49 (2010) 6058–6082.
[4] C.E. Powell, G.G. Qiao, Polymeric CO_2/N_2 gas separation membranes for the capture of carbon dioxide from power plant flue gases, J. Membr. Sci. 279 (2006) 1–49.
[5] A.F. Ismail, L. David, A review on the latest development of carbon membranes for gas separation, J. Membr. Sci. 193 (2001) 1–18.
[6] U. Mueller, M. Schubert, F. Teich, H. Puetter, K. SchierleArndt, J. Pastre, Metal-organic frameworks–prospective industrial applications, J. Mater. Chem. 16 (2006) 626–636.
[7] D. Tanaka, S. Kitagawa, Template effects in porous coordination polymers, Chem. Mater. 20 (2008) 922–931.
[8] P. Bernardo, E. Drioli, G. Golemme, Membrane gas separation: a review/state of the art, Ind. Eng. Chem. Res. 48 (2009) 4638–4663.
[9] A. Gabelman, S.-T. Hwang, Hollow fiber membrane contactors, J. Membr. Sci. 159 (1999) 61–106.
[10] J. Li, B. Chen, Review of CO_2 absorption using chemical solvents in hollow fiber membrane contactors, Sep. Purif. Technol. 41 (2005) 109–122.
[11] K. Simons, K. Nijmeijer, M. Wessling, Gas-liquid membrane contactors for CO_2 removal, J. Membr. Sci. 340 (2009) 214–220.
[12] L.A. Neves, J.G. Crespo, I.M. Coelhoso, Gas permeation studies in supported ionic liquid membranes, J. Membr. Sci. 357 (2010) 160–170.
[13] S. Majumdar, A.K. Guha, K.K. Sirkar, A new liquid membrane technique for gas separation, AIChE J. 34 (1988) 1135–1145.
[14] A.B. Shelekhin, I.N. Beckman, Gas separation processes in membrane absorber, J. Membr. Sci. 73 (1992) 73–85.
[15] M. Poloncarzova, J. Vejrazka, V. Vesely, P. Izak, Effective purification of biogas by a condensing-liquid membrane, Angew. Chem. Int. Ed. 50 (2011) 669–671.
[16] M. Kárászová, J. Vejražka, V. Veselý, K. Friess, A. Randová, V. Hejtmánek, L. Brabec, P. Izák, A water-swollen thin film composite membrane for effective upgrading of raw biogas by methane, Sep. Purif. Technol. 89 (2012) 212–216.
[17] A.K. Geim, Graphene: Status and prospects, Science 324 (2009) 1530–1534.
[18] A. Hashimoto, K. Suenaga, A. Gloter, K. Urita, S. Iijima, Direct evidence for atomic defects in graphene layers, Nature 430 (2004) 870–873.
[19] M.D. Fischbein, M. Drndic, Electron beam nanosculpting of suspended graphene sheets, Appl. Phys. Lett. 93 (2008) 113107.
[20] M.E. Suk, N.R. Aluru, Water transport through ultrathin graphene, J. Phys. Chem. Lett. 1 (2010) 1590–1594.
[21] K. Sint, B. Wang, P. Kra, Selective ion passage through functionalized graphene nanopores, J. Am. Chem. Soc. 130 (2008) 16448–16449.
[22] D. Jiang, V.R. Cooper, S. Dai, Porous graphene as the ultimate membrane for gas separation, Nano Lett. 9 (2009) 4019–4024.
[23] T.R. Gaborski, J.L. Snyder, C.C. Striemer, D.Z. Fang, M. Hoffman, P.M. Fauchet, J.L. McGrath, High-performance separation of nanoparticles with ultrathin porous nanocrystalline silicon membranes, ACS Nano 4 (2010) 6973–6981.
[24] M. Lísal, Z. Posel, P. Izák, Air-liquid interface of imidazolium-based[TF_2N^-] ionic liquids: insight from molecular dynamics simulations, Phys. Chem. Chem. Phys. 14 (2012) 5164–5177.
[25] A.I. Skoulidas, D.M. Ackerman, J.K. Johnson, D.S. Sholl, Rapid transport of gases in carbon nanotubes, Phys. Rev. Lett. 89 (2002) 185901.
[26] M. Majumder, N. Chopra, R. Andrews, B.J. Hinds, Nanoscale hydrodynamics: enhanced flow in carbon nanotubes, Nature 438 (2005) 44.
[27] S. Joseph, N.R. Aluru, Why are carbon nanotubes fast transporters of water? Nano Lett. 8 (2008) 452–458.
[28] W.L. Jorgensen, D.S. Maxwell, J. Tirado-Rives, Development and testing of the OPLS all-atom force field on conformational energetics and properties of organic liquids, J. Am. Chem. Soc. 118 (1996) 11225–11236.
[29] D. Bratko, A. Luzar, Attractive surface force in the presence of dissolved gas: A molecular approach, Langmuir 24 (2008) 1247–1253.
[30] J. Jiang, S.I. Sandler, Nitrogen and oxygen mixture adsorption on carbon nanotube bundles from molecular simulation, Langmuir 20 (2004) 10910–10918.
[31] C.S. Murthy, K. Singer, I.R. McDonald, Interaction site models for carbon dioxide, Mol. Phys. 44 (1981) 135–143.
[32] J.G. Harris, K.H. Yung, Carbon dioxide's liquid-vapor coexistence curve and critical properties as predicted by a simple molecular model, J. Phys. Chem. 99 (1995) 12021–12024.
[33] K.P. Travis, K.E. Gubbins, Transport diffusion of oxygen-nitrogen mixtures in graphite pores: A nonequilibrium molecular dynamics (NEMD) study, Langmuir 15 (1999) 6050–6059.
[34] Y. Miyano, Molecular simulation with an EOS algorithm for vapor-liquid equilibria of oxygen and ethane, Fluid Phase Equilib. 158 (1999) 29–35.
[35] E.J. Maginn, A.T. Bell, D.N. Theodorou, Transport diffusivity of methane in silicalite from equilibrium and nonequilibrium simulations, J. Phys. Chem. 97 (1993) 4173–4181.
[36] T. Somasundaram, R.M. Lynden-Bell, C.H. Patterson, The passage of gases through the liquid water/vapour interface: A simulation study, Phys. Chem. Chem. Phys. 1 (1999) 143–148.
[37] H.J.C. Berendsen, J.R. Grigera, T.P. Straatsma, The missing term in effective pair potentials, J. Phys. Chem. 91 (1987) 6269–6271.
[38] G. Chen, Y. Guo, N. Karasawa, W.A. Goddard III, Electron-phonon interactions and superconductivity in K_3C_{60}, Phys. Rev. B 48 (1993) 13959.
[39] S. Nosé, A molecular dynamics method for simulations in the canonical ensemble, Mol. Phys. 52 (1984) 255–268.
[40] B. Hess, C. Kutzner, D. van der Spoel, E. Lindahl, Gromacs 4, load-balanced, and scalable molecular simulation: algorithms for highly efficient, J. Chem. Theory Comput. 4 (2008) 435–447.
[41] R. Kjellander, S. Marčelja, Perturbation of hydrogen bonding in water near polar surfaces, Chem. Phys. Lett. 120 (1985) 393–396.
[42] B.L. de Groot, H. Grubmüller, Water permeation across biological membranes: mechanism and dynamics of aquaporin-1 and glpf, Science 294 (2001) 2353–2357.
[43] B. Widom, Some topics in the theory of fluids, J. Chem. Phys. 39 (1963) 2808.
[44] D. Frenkel, B. Smit, Understanding Molecular Simulation-From Algorithms to Applications, 2nd ed., Academic Press, San Diego, 2001.
[45] D. Paschek, Temperature dependence of the hydrophobic hydration and interaction of simple solutes: an examination of five popular water models, J. Chem. Phys. 120 (2004) 6674.
[46] C. Matranga, L. Chen, M. Smith, E. Bittner, J.K. Johnson, B. Bockrath, Trapped CO_2 in carbon nanotube bundles, J. Phys. Chem. B 107 (2003) 12930–12941.
[47] A. Alexiadis, S. Kassinos, Molecular dynamic simulations of carbon nanotubes in CO_2 atmosphere, Chem. Phys. Lett. 460 (2008) 512–516.